Available online at www.sciencedirect.com
SCIENCE DIRECT®
International Journal of Multiphase Flow 32 (2006) 208–231
International Journal of Multiphase Flow
www.elsevier.com/locate/ijmulflow

Experimental study of pool temperature effects on nucleate pool boiling

Jeongbae Kim [a], Byung Do Oh [b], Moo Hwan Kim [b,*]

[a] New and Renewable Energy Research Department, KIER (Korea Institute of Energy Research), 71-2, Jang-dong, Yuseong-gu, Daejeon 305-343, Republic of Korea
[b] Department of Mechanical Engineering, Pohang University of Science and Technology, San 31, Hyoja-dong, Namgu, Pohang, Kyoungbuk 790-784, Republic of Korea

Received 28 December 2004; received in revised form 15 September 2005

Abstract

Nucleate pool boiling experiments with constant wall temperature were performed using pure R113 for subcooled, saturated, and superheated pool conditions. A microscale heater array and Wheatstone bridge circuits were used to maintain the constant wall temperature and to measure the instantaneous heat flow rate accurately with high temporal and spatial resolutions. Images of bubble growth were taken at 5000 frames per second using a high-speed CCD camera synchronized with the heat flow rate measurements. The bubble geometry was obtained from the captured bubble images. The effect of the pool conditions on the bubble growth behavior was analyzed using dimensionless parameters for the initial and thermal growth regions. The effect of the pool conditions on the heat flow rate behavior was also examined. The bubble growth behaviors during subcooled, saturated, and superheated pool boiling were analyzed using a modified Jakob number that we newly defined. Dimensionless time and bubble radius parameters with the modified Jakob number characterized the bubble growth behavior well. These phenomena require further analysis for various pool temperature conditions, and this study will provide good experimental data with precise constant wall temperature boundary condition for such works.

Keywords: Pool temperature; Constant wall temperature; Single bubble growth; Nucleate pool boiling; Microscale heater array

1. Introduction

Many experiments and analyses have been performed to clarify the heat transfer mechanism of boiling. The overall characteristics of boiling are directly and indirectly influenced by the behavior of a single bubble on the heating surface. The heat transfer mechanism for single bubble growth can be related to the thermal boundary layer characteristics on the heating surface. These are controlled by the wall and pool temperatures during the

* Corresponding author. Tel.: +82 54 279 2165; fax: +82 54 279 3199.
E-mail address: mhkim@postech.ac.kr (M.H. Kim).

0301-9322/$ - see front matter © 2005 Elsevier Ltd. All rights reserved.
doi:10.1016/j.ijmultiphaseflow.2005.09.005

waiting period, and by the interface temperature gradient, which is depended on wall, saturation, and pool temperatures during the growth time. Consequently, the temperature scales closely connected to nucleate pool boiling are the pool temperature (subcooled, saturated, and superheated), saturation temperature of the working fluid, and heating wall temperature.

Rayleigh (1917) proposed the momentum equation for a spherical bubble to be governed by the momentum interaction between the two phases without considering the heat transfer through the interface between the liquid and vapor bubble. Analytically, he showed that bubble radius was proportional to the growth time based on a constant pressure difference assumption. Plesset and Zwick (1954) and Forster and Zuber (1954) analyzed the extended Rayleigh equation considering the heat transfer through the bubble interface in a uniformly superheated liquid, and then derived a bubble growth equation using heat conduction through the thermal boundary layer. They assumed a thin thermal boundary layer and uniformly superheated liquid surrounding the vapor bubble, and derived the temperature distribution at the interface. Their analysis showed that the bubble radius increased proportionally with $t^{1/2}$. For a vapor bubble larger than a critical radius and surrounded by a uniformly superheated liquid, Mikic et al. (1970) analyzed the bubble growth behavior using characteristic length and time scales in a dimensional analysis. They reported that the bubble radius increased proportionally with t^1 for dimensionless time values much less than 1 ($t^+ \ll 1$), and with $t^{1/2}$ for dimensionless time values much greater than 1 ($t^+ \gg 1$). However, they did not categorize the bubble growth regions.

Robinson and Judd (2001) performed a numerical simulation of bubble growth based on interface temperature calculations using the extended Rayleigh and energy equations. They considered the inside vapor pressure of a hemispherical bubble attached on the heating surface and demonstrated that heat transfer occurred through the bubble interface due to the interface cooling effect previously proposed by Plesset and Zwick (1954), Zuber (1961), and Mikic et al. (1970). They divided the bubble growth regions based on their numerical results. When a bubble forms after a waiting period, the bubble growth is governed by the surface tension for a short period of time (surface-tension controlled region). As the bubble increases in volume, the surface tension is reduced while the inertia is increased (inertia controlled region). When the vapor pressure of the bubble is balanced with the system pressure, the temperature distribution at the interface of the two phases becomes the most important parameter for bubble growth (thermal growth region).

According to bubble radius results of Han and Griffith (1965) and Cole and Shulman (1966), performed at a constant heat flux condition for saturated pool boiling, there are the large deviations even when tests are performed under the same experimental conditions. These arise from the poor control capacity of the heating surface. Our analysis showed that the control speed of the heating surface must be only a few microseconds to maintain a constant heating condition from bubble inception to departure. Hooper and Abdelmessih (1966) and Sernas and Hooper (1969) performed nucleate pool boiling experiments using water with a constant heat flux condition and then studied the bubble growth behavior during the initial growth region. However, they compared their experimental results with the growth rate of $t^{1/2}$ obtained from the analytical results of Plesset and Zwick (1954) and Forster and Zuber (1954).

And previously, Lee et al. (2003b) reported that the growth rate in the thermal growth region varied as $t^{1/7}$ with the bubble growth result at only one wall superheat condition for saturated pool condition using R11, but fixed in the initial growth rate like t^1 as the propose of Rayleigh (1917). Then, Lee et al. (2003a) demonstrated that the bubble growth rate in the thermal growth region followed as $t^{1/5}$ with various wall superheats for just saturated pool condition using R11 and R113, but fixed in the initial growth rate with t^1 as proposed by Rayleigh (1917). They used a Jakob number (Ja) based on the wall superheat (the difference between the wall and saturation temperatures) ranging from 14 to 21. Also reported that the thermal growth rate was regardless of the working fluid and heating conditions. Lee et al. (2004) showed that the growth behavior of binary mixtures in the thermal growth region for saturated pool condition was almost same as for pure substances.

In this study, we performed nucleate pool boiling experiments with fixed wall temperature using one fluid to examine pool temperature effects on the bubble growth behavior. In previous studies, it was almost impossible to maintain a constant fixed wall temperature for nucleate pool boiling under constant atmospheric pressure condition. Even for saturated and subcooled pool boiling, the heating surface condition used in most previous single bubble growth research was a constant heat flux that could be obtained by heating a metallic block installed below the bubble. There were large deviations in the bubble radius results of Han and Griffith

(1965), Cole and Shulman (1966), and Zuber (1961), even when the experiments were performed under the same conditions. This resulted from the poor control capacity of the heating surface. A control speed of a few microseconds is required to respond to the local heating conditions and a fixed temperature during bubble formation.

Zuber (1961) proposed a growth and collapse equation using the maximum bubble radius and time under non-uniform temperature fields based on subcooled nucleate boiling results of Ellion. Demiray and Kim (2003) described the bubble growth behavior for subcooled boiling at 5 °C (low amount) and 15 °C (high amount) of subcooling under constant temperature condition using FC-72 ($T_{sat} = 56.7$ °C). In addition, Kim et al. (2002) published the effects of subcooling on the pool boiling heat transfer. However they did not fully describe the effects of the pool temperature on the bubble growth behavior.

For superheated pool condition, previous studies usually performed at an infinite pool, so that during growth, the bubble was not attached to the heating surface and there was no effect due to the waiting period between series of bubbles from inception to departure. Forster and Zuber (1954), Dergarabedian (1960), and Saddy and Jameson (1971) presented bubble growth rate and heat transfer results that considered the pool superheat effect at an infinite pool of water at atmospheric pressure. Their experimental pool conditions from 1 to 5 °C of pool superheat. Lien (1969) performed a similar study to study the bubble growth rate for 9–16 °C of superheat with a variable system pressure and an infinite pool. Van Stranlen et al. (1975) studied the growth rate of a bubble attached to the heating surface until departure in a pool with 0.8–2.3 °C of superheat, also with a variable system pressure.

The objective of this study was to investigate the effect of only pool temperature conditions (superheated, saturated, and subcooled) on single bubble growth characteristics including bubble growth rates in initial and thermal growth regions under constant wall temperature and atmospheric pressure. To do so, the wall temperature was fixed using a microscale heater array with high temporal and spatial resolutions that was originally designed by Rule et al. (1998), Lee et al. (2003a,b) used the same microscale heater array.

To achieve our objective, nucleate pool boiling experiments were conducted for subcooled, saturated, and superheated pool conditions using pure R113 ($T_{sat} = 47.6$ °C). The wall temperature was maintained at a 72 °C for all the pool temperature conditions. For subcooled conditions, the pool temperature was set to 30, 32, 34, 36, 38, 40, 42, 44, and 45 °C to consider and include the subcooled range of Demiray and Kim (2003). For superheated conditions, the pool temperature was set to 48, 49, and 50 °C. A pool temperature of 47 °C was considered as nearly saturated and used as the reference condition. When the pool temperature exceeded 50 °C and was lower than 30 °C, regular single bubble events did not occur; therefore, we could not obtain bubble images or measure the heat flow rate with a good degree of repeatability.

2. Experiments

2.1. Experimental apparatus

We used a microscale heater array to maintain a constant temperature at the heating surface and to measure the heat flow rate. The heater was fabricated on a transparent glass wafer using a very-large-scale-integrated (VLSI) technique. The transparency provided a bottom view of the growing bubble, which was captured using a high speed CCD camera. First, a titanium and platinum layer for the heater line on the wafer was installed using thermal evaporation. Then, a titanium and platinum layer for the power line was fabricated. The roughness of the heating surface was approximately 0.4 μm, which was the height of the heating line with respect to the base substrate. The static contact angle of the microscale heater array surface was 71° for distilled water and 11.4° for R113, which indicates the hydrophilic nature of R113. A total of 96 microscale heaters comprised one microscale heater array. Each microscale heater measured 0.27×0.27 mm^2, and the total size of the microscale heater array was 2.7×2.7 mm^2. For our experiments, the heater was manufactured at the Samsung Advanced Institute of Technology based on the idea of Rule et al. (1998) and Rule and Kim (1999). Most of the experimental devices that have been used previously to control the power of the heating block beneath the bubble, and thereby provide a constant heat flux, could not maintain a constant surface temperature over very short time intervals. However, our microscale heater array was controlled with a Wheatstone bridge circuit that provided a constant surface temperature with a high temporal resolution.

The longest time delay in the circuit occurred at the OP amp, which had a time resolution of 10^{-7} s. Due to the fast response of the circuitry, good repeatability was achieved in our experimental results.

To maintain and control the constant temperature condition, each heater was previously calibrated for temperatures ranging from 20 to 80 °C. The temperature of the 96 heaters in the array was controlled by 96 electric Wheatstone bridge feedback circuits, which were operated in a manner similar to that used for constant-temperature hot-wire anemometry. Each heater in the array could be represented as one resistor in a Wheatstone bridge circuit. The calibration process for the wall temperature of the heater was described in Lee et al. (2003a,b). A data acquisition system, which could measure and store data at 7.35 kHz with 12-bit resolution, was used to measure the heat flow rate of each heater throughout the experiments. Therefore, the voltage data for each heater was sampled every 0.136 ms, and 1000 voltage readings for each heater were stored with the 12-bit resolution. All the tests performed in this study lasts 136 ms. These measurements were synchronized with the images captured by the high speed CCD camera. A more detail description can be found in Rule and Kim (1999) and Bae et al. (1999). Fig. 1 shows a schematic diagram of the experimental apparatus. Ten thin film heaters with 15,500 W/m^2 were used to control the liquid temperature inside the test chamber as close to the saturation temperature as possible without providing another heat source for the bubble. A 150 W cold light source was used for the CCD camera. The speed of CCD camera (Redlake Co., HG-100K) was 5000 frames per second. A long distance microscopic lens was used to capture the small bubbles during boiling (see Fig. 1).

2.2. Uncertainty analysis

The bubble growth behavior was analyzed using side-view images, while the heat flow rate measured using the microscale heater during growth. Since most previous results for bubble growth have been for a spherical bubble, the growth behavior in this study was analyzed using the equivalent radius of a sphere with the same volume. The captured images showed reasonable bubble geometries, with an axi-symmetric shape about the vertical axis and a non-symmetric shape about the horizontal axis, as shown like Fig. 2. (Kim et al. (2004a,b)) Based on the shape assumption, we calculated the volume of upper and lower parts of the bubble using

$$V_{\mathrm{U}} = \frac{2}{3}\pi B^2 A \tag{1}$$

$$V_{\mathrm{L}} = \pi B^2\left[D - \frac{D^3}{3E^2}\right], \quad E = \sqrt{\frac{D^2}{1-\frac{(C/2)^2}{B^2}}} \tag{2}$$

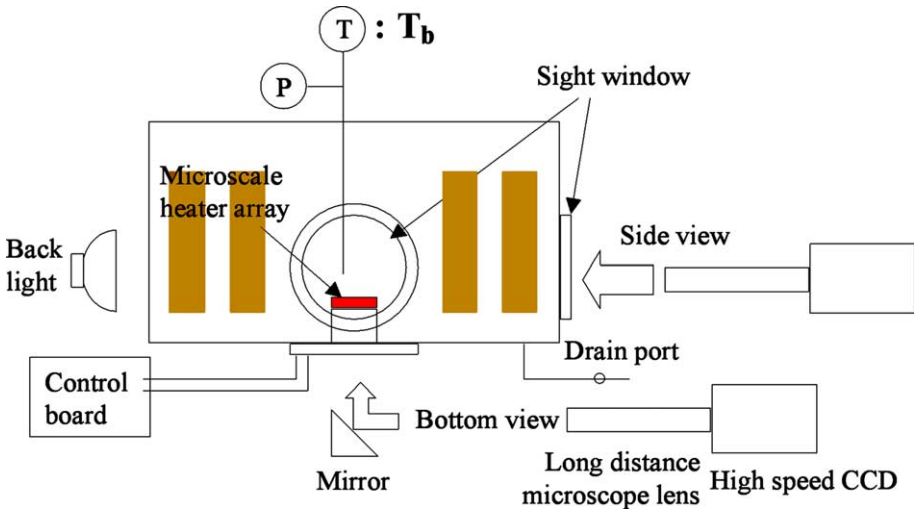

Fig. 1. Schematic diagram of the experimental apparatus.

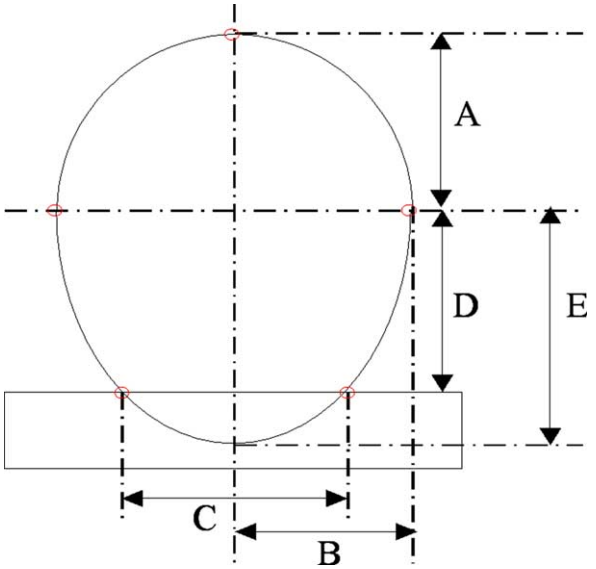

Fig. 2. Geometry of the spheroid used to determine the bubble volume.

where, A, B, C, D and E are the dimensions indicated in Fig. 2. V_U is the volume of the upper part of the bubble, and V_L is the volume of the lower part of the bubble. V_L can also be calculated using B, D, and C (see Fig. 2). The equivalent radius, R_{eq}, can then be defined as the radius for which the total volume (V) from the measurements is balanced with that of a sphere with an equivalent radius

$$V = V_U + V_L = \frac{4}{3}\pi R_{eq}^3 \tag{3}$$

$$R_{eq} = \left(\frac{1}{2}B^2A + \frac{3}{4}B^2\left[D - \frac{D^3}{3E^2}\right]\right)^{\frac{1}{3}} \tag{4}$$

The heat flow rate supplied to the bubble corresponds to that required for the total bubble volume change based on the assumption that the volume change is induced by latent heat transfer. This can be calculated from

$$\dot{q} = \dot{m}h_{fg} = 4\pi\rho_v h_{fg} R^2 \frac{dR}{dt} \tag{5}$$

Here, $\dot{q}$ is the heat flow rate, $\dot{m}$ is the evaporating mass flow rate, h_{fg} is the latent heat for vaporization, ρ_v is the vapor density, R is the equivalent bubble radius, and t is time.

The equivalent radius can be calculated from the dimensions shown in Fig. 2; however, the errors in the dimensional measurements will propagate into the calculation of the equivalent radius. The dimensions shown in Fig. 2 were measured by counting the number of pixels in each captured image. A micrometer was placed in the chamber at the same distance as the bubble nucleation to provide guidance for the size measurements. From the captured micrometer images, a physical dimension of 1000 mm corresponded to 197 pixels in our experiments. Therefore, one pixel in each image corresponded to 5.0761 μm. The clearly captured images could be measured with an error of ±1 pixel. An uncertainty analysis was performed using the method described by Coleman and Steele (1989). The maximum uncertainty in the first image, which contained the smallest bubble, was 5.0%.

The bubble inception time was obtained from the time when the first image was recorded as indicated by the CCD camera, and from the heat flow rate data. The images were recorded with a time resolution of 0.2 ms (5000 frames/s). We defined the inception time was as the point immediately before the jump in the recorded heat flow rate data; therefore, the inception time error was a maximum of 0.136 ms. A thermocouple with

0.53 °C uncertainty was used to calibrate the temperature of the microscale heater array. The Wheatstone bridge circuit was set to give a temperature displacement of 60 °C and the digital potentiometer in the Wheatstone bridge circuit had 512 digital positioning numbers. Therefore, one digit had a 0.12 °C temperature displacement and an uncertainty of 0.06 °C. The maximum uncertainty of the calibrated temperature was estimated to be 0.59 °C which was the sum of the errors of the thermocouple and digital potentiometer: 0.53 °C and 0.06 °C, respectively.

The voltage of each heater was measured using a 12-bit A/D system. The maximum voltage was 12 V. Therefore, the digitizing bias error was estimated to be ±0.0015 V. All of the heater output voltages measured while a bubble was generated were above 2 V and the maximum uncertainty of the voltage measurements was ±0.075%.

The temperature difference between the heating wall and pool was a maximum of 40 °C for the subcooled case with a pool temperature of 32 °C. The difference in the refractive index of pure R113 is roughly 0.59% for a temperature difference of 40 °C. The distortion or refraction error caused at the window or near the heating surface liquid, whose density differs from that of the bulk liquid, will be negligible. The data on the refractive index of pure R113 was obtained from page 18.3 of the 1997 Fundamentals of ASHRAE Handbook and page 1640 of the Handbook of Fine Chemicals and Laboratory Equipment of Aldrich (2001).

3. Results and discussion

3.1. Measured heat flow rate uncertainty and bubble geometry

One of our objectives was to analyze the growth behavior of a single bubble by measuring the heat flow rate supplied from the heating wall under constant wall temperature condition for each pool temperature. Therefore, the uncertainty of the measured heat flow rate at the microscale heater is important. To evaluate the uncertainty of all the experiments conducted in this study, we examined the measured heat flow rate behavior in Fig. 3. Fig. 3 shows the heat flow rate behavior of the measured cycles for 32, 42, 47, and 49 °C. The maximum error arises from the 0.136 ms in the bubble inception time measurements due to the time resolution of the heat flow rate. After an initial peak and an abrupt decrease, the heat flow rates showed good repeatability with deviations of 4%. This suggests that the bubble behavior will be similar for each period between inception and departure.

In order to verify the assumed bubble geometry, which was used to obtain the equivalent bubble radius, we inspected the bubble shapes during growth using captured image, such as those shown in Fig. 4. The images showed bubbles that were almost axi-symmetric about the axis normal to the heating surface, but not symmetric about the horizontal axis, regardless of the pool temperature conditions. These images were compared to the bubble geometry illustrated in Fig. 2. A necking phenomenon occurred close to the departure time, resulting in a difference between the assumed shapes and the actual images. The maximum difference appeared right at the departure time. To evaluate the equivalent radius of the actual bubble, the coordinates of the bubble interface were measured and integrated to obtain the volume. The equivalent radius evaluated from the actual volume at the departure time for a pool temperature of 47 °C pool temperature was 0.589 mm, and the equivalent radius evaluated from the assumed shape at the same time was 0.612 mm. Therefore, the estimated maximum error in the assumed shape was 3.8%.

Fig. 5 gives values of the dimensions A, B, C, and D, which were illustrated in Fig. 2 for bubbles under various pool conditions. Here, A is the height of the upper part, B is the maximum radius, C is the contact diameter, and D is the height of the lower part. Except for a pool temperature of 32 °C, which was a highly subcooled case, the characteristics of the bubble geometries for different pool conditions were very similar.

The estimated equivalent bubble radius for each pool temperature is shown in Fig. 6. Fig. 6 indicates that the larger bubble, the greater the pool temperature. For subcooled conditions ranging from 38 to 45 °C, the bubble radius did not decrease until departure, although the pool temperature was less than the saturation temperature. The bubble radius decreased for pool temperatures less than 36 °C, and a negative growth rate was observed for pool temperatures of 32 and 34 °C. For superheated conditions ranging from 48 to 49 °C, the bubble growth rate was greater than that of the almost saturated case at 47 °C.

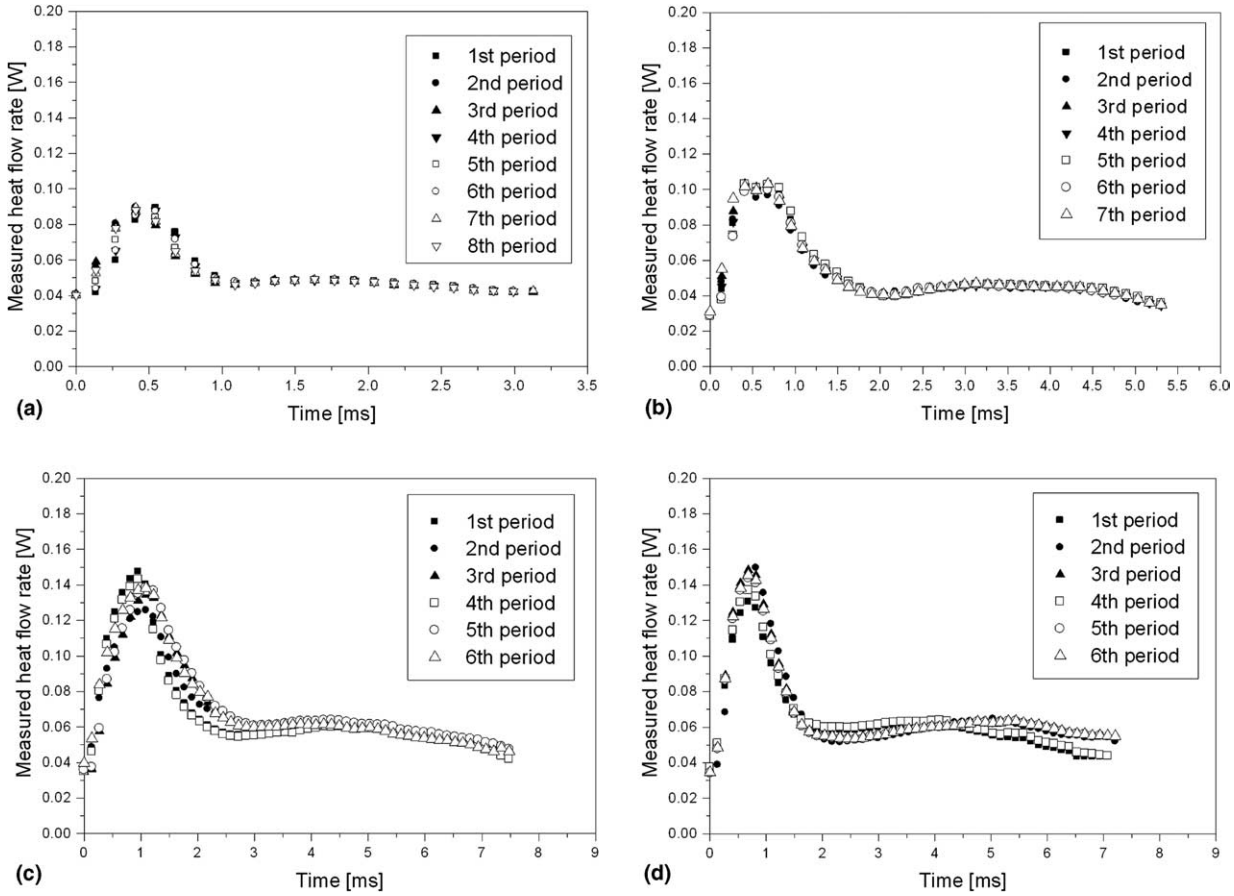

Fig. 3. Repeatability of the measured heat flow rate: (a) $T_b = 32$ °C, (b) $T_b = 42$ °C, (c) $T_b = 47$ °C and (d) $T_b = 49$ °C.

The equivalent radius of the saturated pool condition with a temperature of 47 °C is compared wirh previous analytical results in Fig. 7(a). Plesset and Zwick (1954) assumed a uniformly superheated thermal boundary layer around the spherical bubble and predicted a $t^{1/2}$ asymptotic growth rate. Other predictions that modified using the effective heat transfer area (Van Stralen, 1966) and considered the non-uniform temperature field around the bubble (Mikic and Rohsenow, 1969) still give that the bubble grows with an asymptotic growth rate of approximately $t^{1/2}$. However, our results showed two different regions between bubble inception and departure. Before 1 ms, the growth rate in the initial growth region was proportional to $t^{2/3}$, as proposed by Kim et al. (2004a,b); after 1 ms, the growth rate in the thermal growth region was much slower and was proportional to $t^{1/5}$, as described by Lee et al. (2003a,b).

The power of time for bubble growth is intimately related to the heat flow rate behavior. If the power of time for bubble growth is less than one-third, the heat flow rate described by Eq. (5) will decrease. Therefore, during the initial growth region, when the power of the growth rate was 2/3 (see Fig. 7(a)), the heat flow rate increased with time (see Fig. 7(b)). By contrast, during the thermal growth region, when the power of the growth rate was 1/5 (see Fig. 7(a)), the heat flow rate decreased with time (see Fig. 7(b)).

The equivalent radius obtained for pool temperatures of 32, 38, 42, and 49 °C is compared with the analytical results of Mikic and Rohsenow (1969) and Zuber (1961) in Fig. 8. In the initial growth region, the growth rate was proportional to $t^{2/3}$, as proposed by Kim et al. (2004a,b) for saturated pool condition. Nevertheless, the growth rate in the thermal growth region was quite different from that obtained for saturated condition.

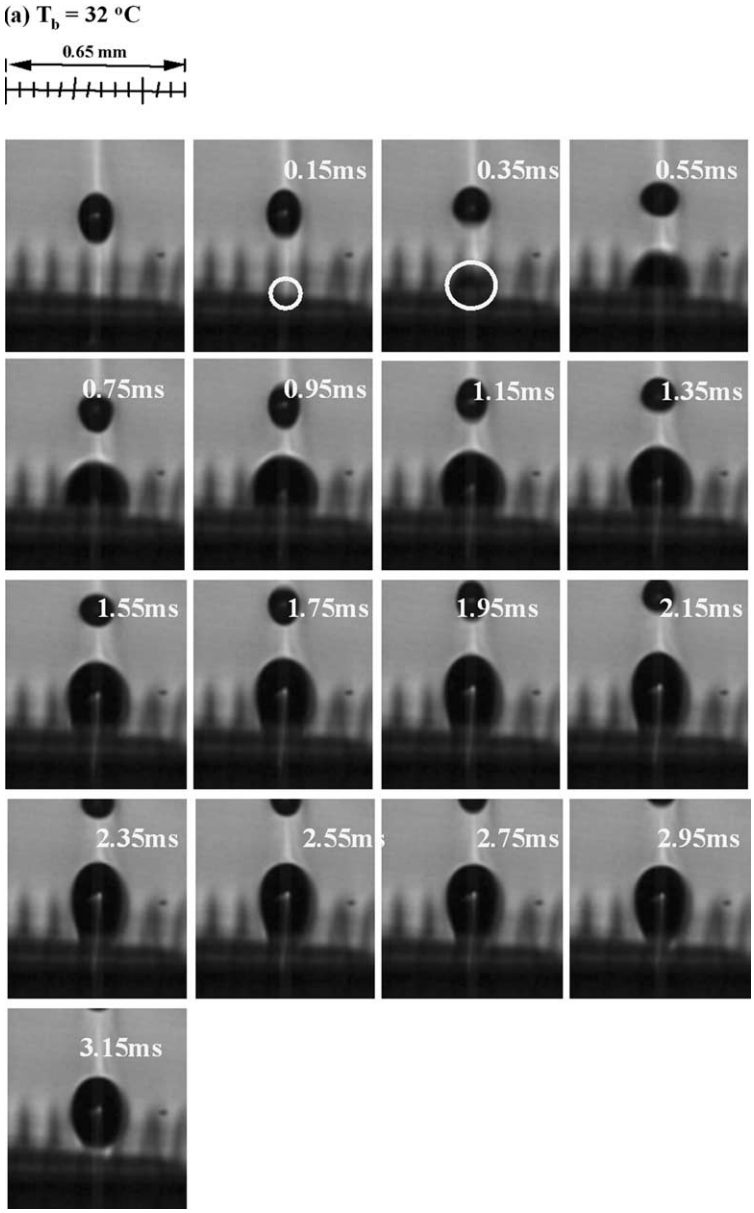

Fig. 4. Side view images of bubble growth ((a) $T_b = 32$ °C and (b) $T_b = 47$ °C).

3.2. Waiting and growth time

The waiting time was maximal for a pool temperature of 42 °C, and was affected by the amount of liquid flowing into the vacant volume after departure and the temperature of that liquid flowed, as illustrated in Fig. 8. The growth time was dependent on the departure mechanism, and the departure time depended on the contact radius at departure. It was difficult to estimate the contact radius at departure because of the time gap between the capturing bubble images. Therefore, it was difficult to explain the relationship between the growth time and pool temperature. Nevertheless, as shown in Fig. 9, the growth time increased with the radius at departure time.

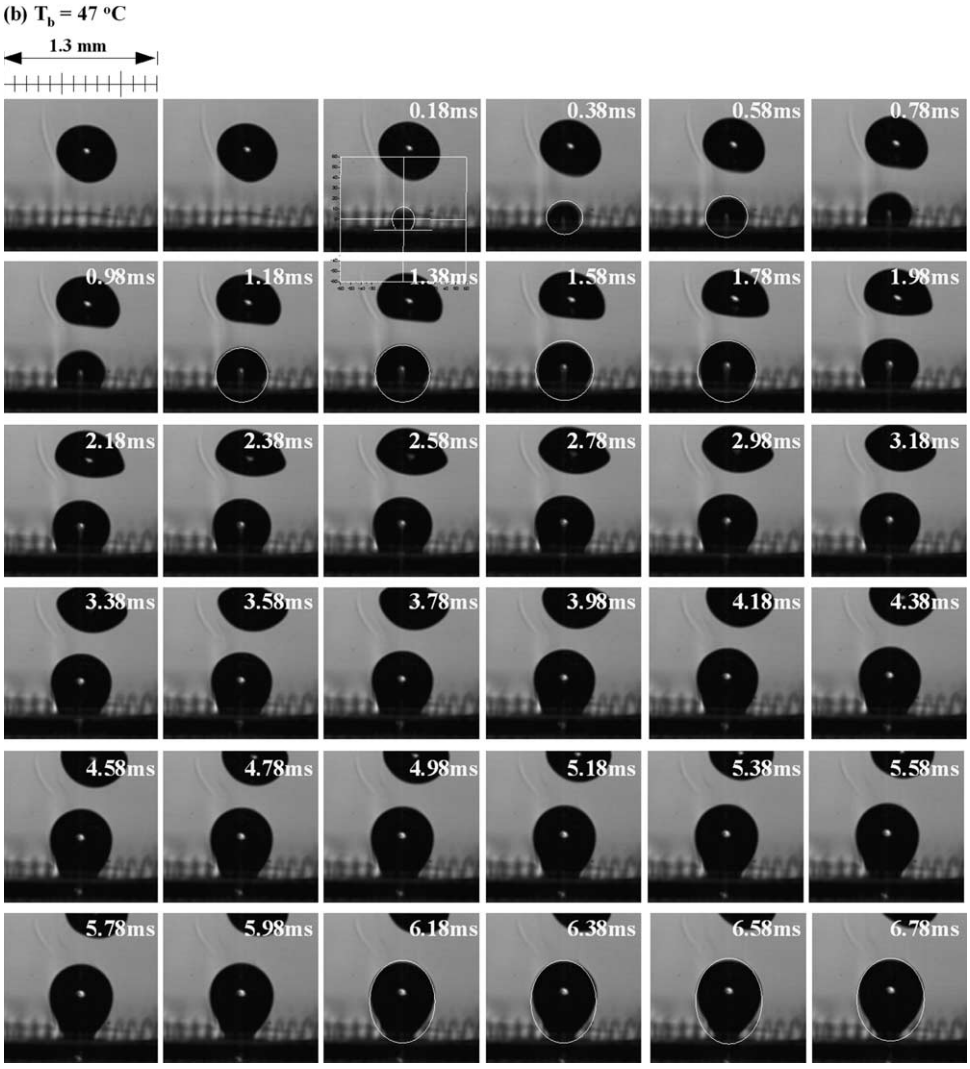

Fig. 4 (*continued*)

3.3. Dimensional analysis of the bubble growth

Suppose that the bubble growth can be characterized by the pressure difference (ΔP) between the vapor and the bulk liquid pressures. Then, the characteristic velocity scale (v_c) can be determined from the driving potential,

$$v_c = \frac{R_c}{t_c} = \sqrt{\frac{2}{3}\frac{\Delta P}{\rho_l}} \tag{6}$$

where R_c is the characteristics bubble radius scale, t_c is the characteristics time scale, and ρ_l is the liquid density.

Here, the factor two-thirds is inserted to allow comparisons with the dimensionless parameter of Mikic et al. (1970).

The bubble growth behavior shown in Fig. 6 is different for each pool temperatures. We performed a dimensional analysis to compare the growth behavior with the same scales of the bubble growth, which required the characteristic time and length scales.

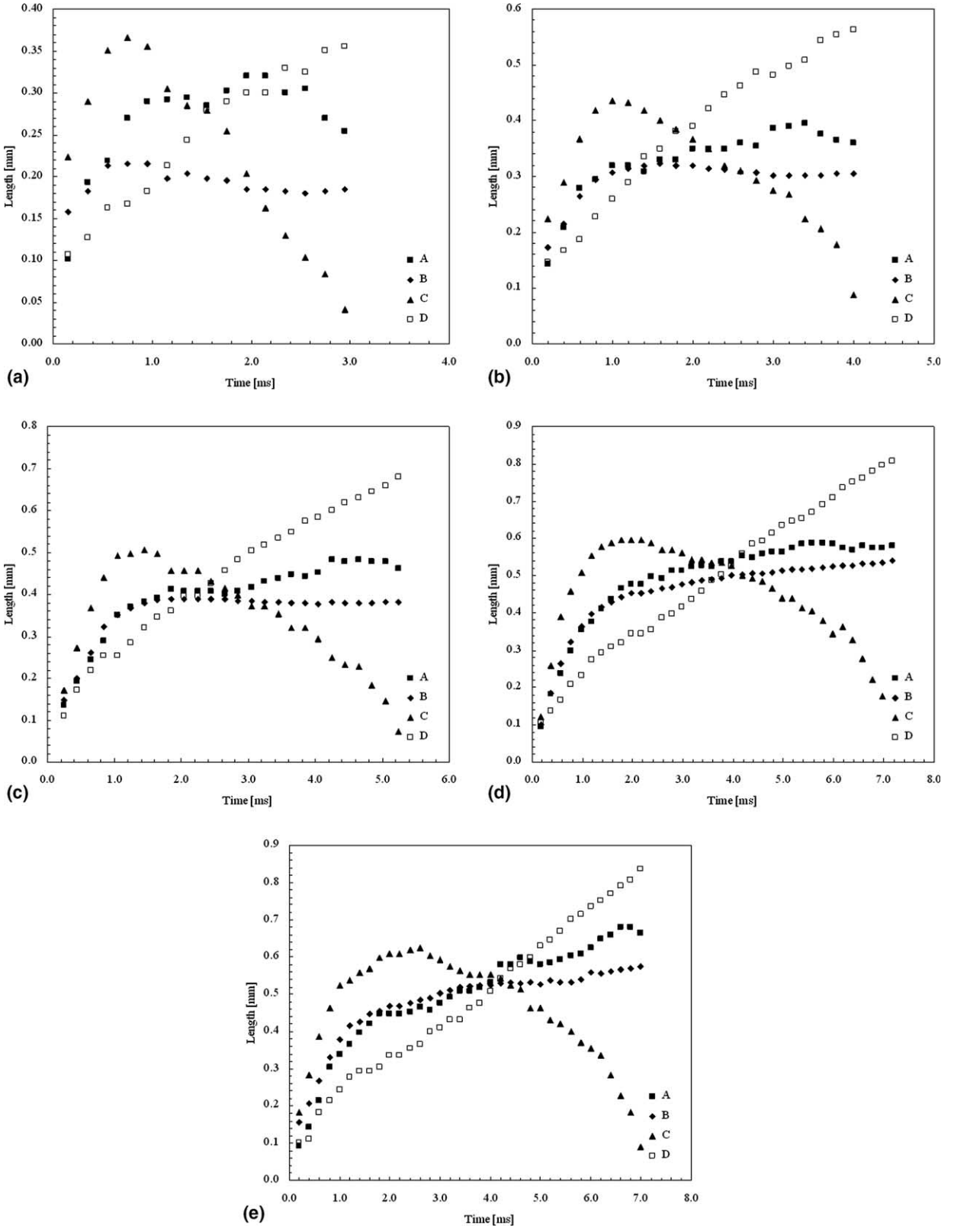

Fig. 5. Bubble geometries for various pool conditions: (a) $T_b = 32$ °C, (b) $T_b = 38$ °C, (c) $T_b = 42$ °C, (d) $T_b = 47$ °C and (e) $T_b = 49$ °C.

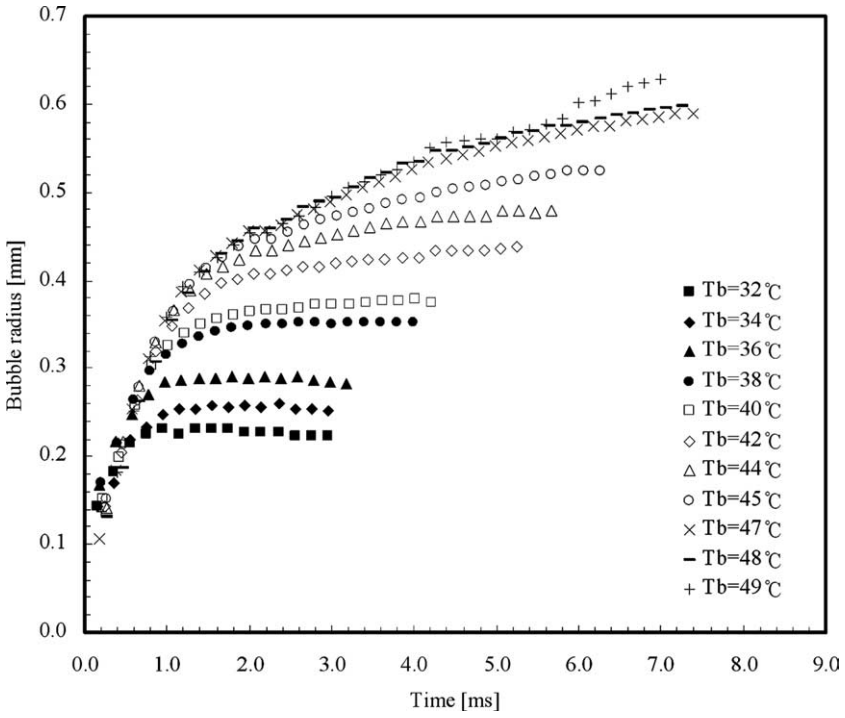

Fig. 6. Equivalent bubble radius for different pool temperatures.

The characteristic time scale can be determined from the ratio of the corresponding latent heat transfer and the conduction heat transfer rate through the interface,

$$\frac{q_{\text{latent}}}{\dot{q}_{\text{conduction}}} = \frac{\rho_v h_{fg} \frac{4}{3}\pi R^3}{k_l 4\pi R^2 \frac{\partial T}{\partial r}} = \frac{1}{3}\frac{\rho_v h_{fg} R_c^3}{k_l R_c^2 \frac{T_c}{R_c}} \frac{R^{+3}}{R^{+2}\frac{\partial T^+}{\partial r^+}} = t_c \frac{R^+}{\frac{\partial T^+}{\partial r^+}} \tag{7}$$

$$t_c = \frac{1}{3}\frac{\rho_v h_{fg} R_c^2}{k_l T_c} = \frac{1}{3}\frac{\rho_v h_{fg} R_c^2}{k_l \Delta T} = \frac{1}{3}\frac{1}{Ja\alpha} R_c^2 \tag{8}$$

where k_l is the thermal conductivity, T is the temperature, and α is the thermal diffusivity of the liquid. Since the bulk liquid is saturated and bubble growth should be influenced by the wall superheat, the Jakob number is defined by $(\rho_l C_{P_l} \Delta T)/(\rho_v h_{fg})$, where the wall superheat ($\Delta T = T_{wall} - T_{sat}$) is used as the characteristic temperature scale (T_c). From Eqs. (6) and (8), the characteristic radius and time scales are

$$R_c = \sqrt{\frac{27}{2}} Ja\,\alpha \sqrt{\frac{\rho_l}{\Delta P}}, \quad t_c = \frac{9}{2} Ja\,\alpha \frac{\rho_l}{\Delta P} \tag{9}$$

Then, the dimensionless bubble radius and time can be expressed as

$$R^+ = \frac{R}{R_c}, \quad t^+ = \frac{t}{t_c} \tag{10}$$

Mikic et al. (1970) assumed that bubble motion is governed by the extended Rayleigh equation

$$\Delta P = P_v - P_\infty = \rho_l R \frac{d^2 R}{dt^2} + \frac{3}{2}\rho_l \left(\frac{dR}{dt}\right)^2 + \frac{2\sigma}{R} \tag{11}$$

By comparing the pressure difference and the second term on the right hand side of the equation, the same characteristic velocity scale can be derived. Furthermore, Mikic et al. (1970) assumed that the pressure difference was constant, and can be replaced by the superheat using the Clausius–Clapeyron relation

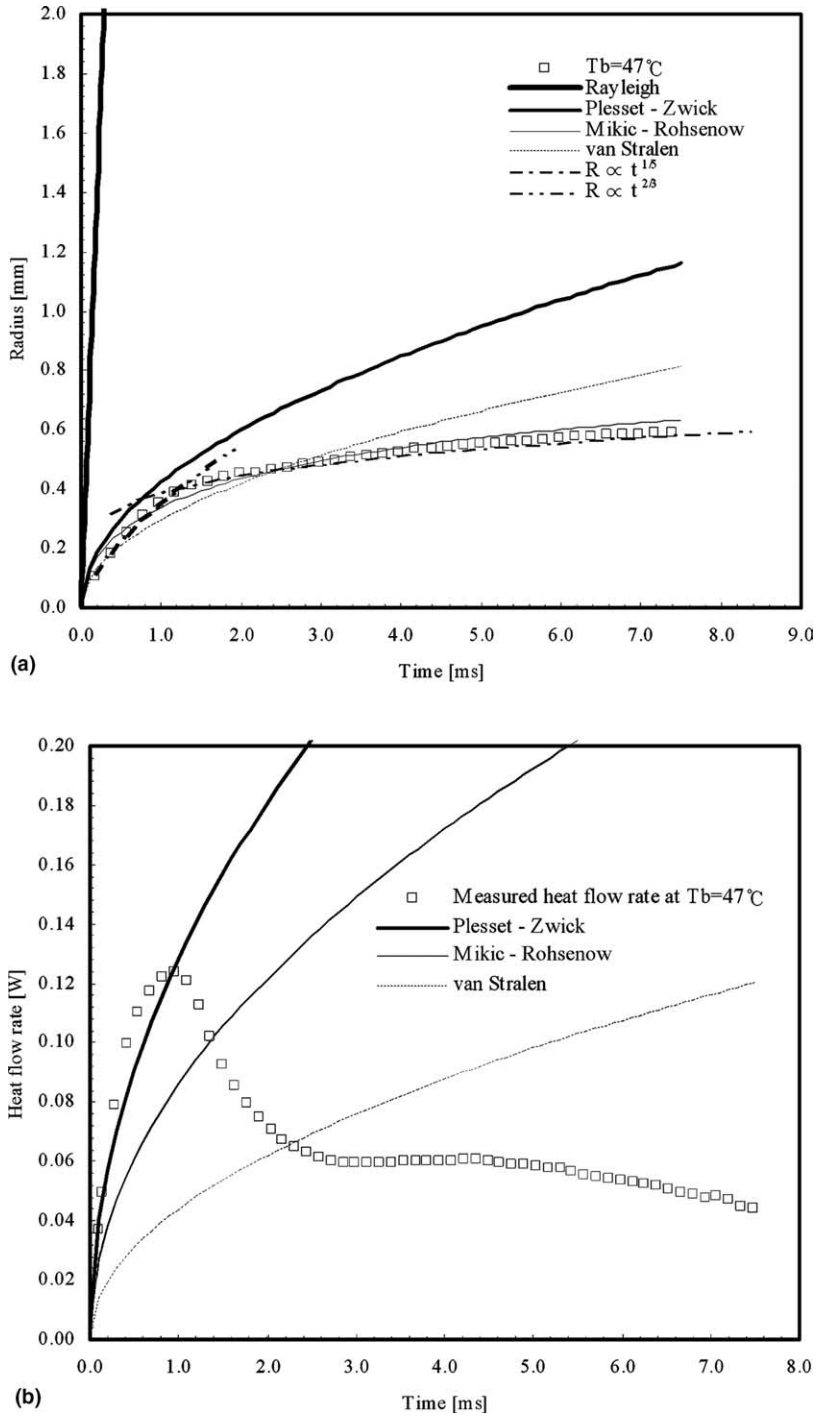

Fig. 7. Comparison of bubble growth with previous predictions ($T_b = 47$ °C).

$$v_c = \frac{R_c}{t_c} = \sqrt{\frac{2}{3}\frac{\Delta P}{\rho_l}} = \sqrt{\frac{2}{3}\frac{\rho_v h_{fg} \Delta T}{\rho_l T_{sat}}} \tag{12}$$

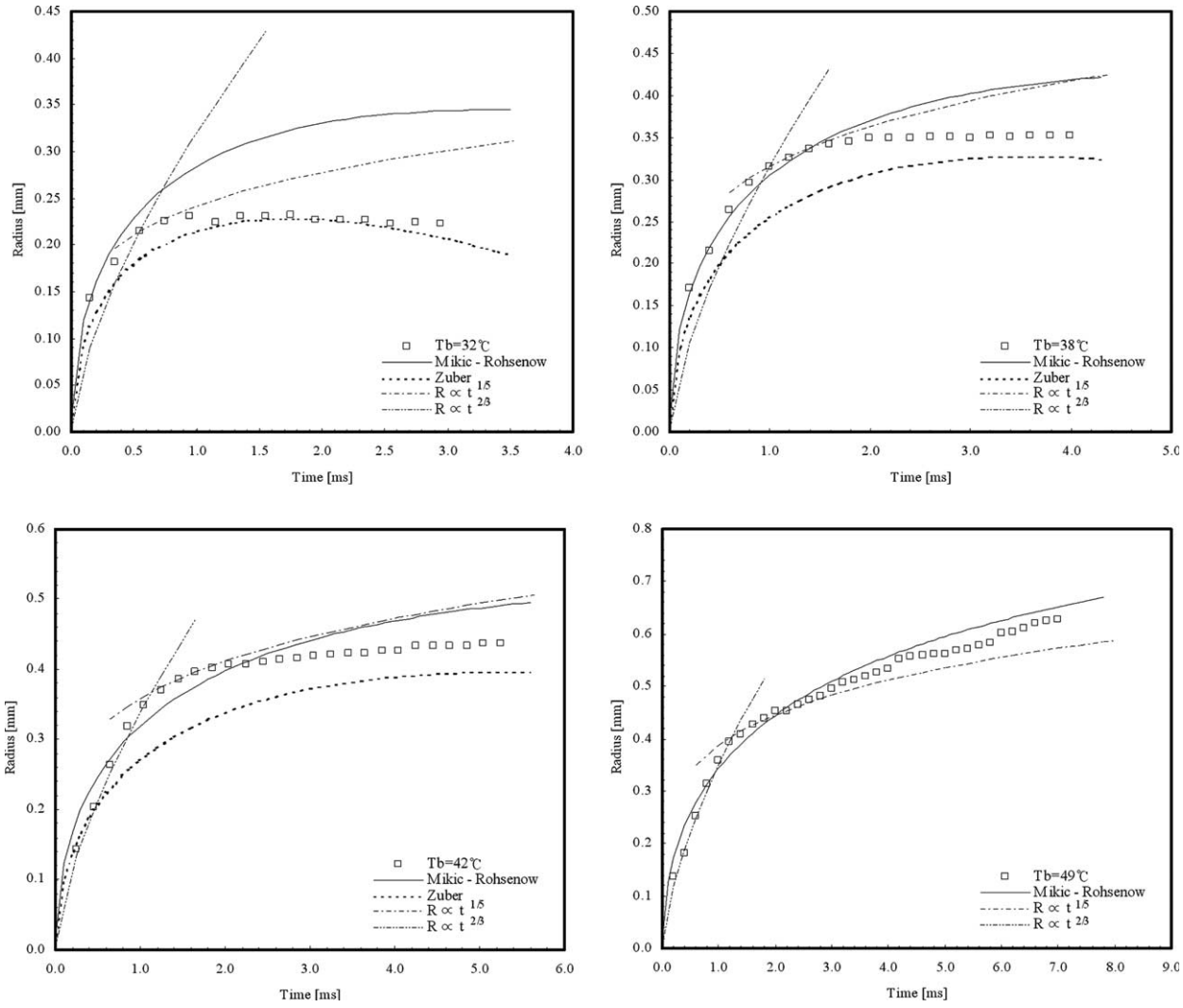

Fig. 8. Comparison of bubble growth with previous predictions ($T_b = 32$, 38, 42, and 49 °C).

where the growth rate of Plesset and Zwick (1954) was also used for the characteristic scale. This suggests the following parameters:

$$R_c = \frac{\frac{12}{\pi} Ja^2 \alpha}{\sqrt{\frac{\pi}{7} \frac{\rho_v h_{fg} \Delta T}{\rho_l T_{sat}}}}, \quad t_c = \frac{\frac{12}{\pi} Ja^2 \alpha}{\frac{\pi}{7} \frac{\rho_v h_{fg} \Delta T}{\rho_l T_{sat}}} \tag{13}$$

It is of interest to note that almost the same relation as Mikic's scaling parameters shown above can be obtained when the critical bubble radius is used to determine the pressure difference in Eq. (12). The critical radius can be obtained using the Clausius–Clapeyron relation and the Laplace–Kelvin equation for static equilibrium. Therefore, the scaling parameters in Eq. (13) adequately describe the initial growth behavior, but not the asymptotic behavior (in the thermal controlled region).

We will use the departing radius as a scaling parameter to adjust for the thermal growth behavior. The pressure difference can be related to the departing radius, R_d, using the static equilibrium since the radial acceleration and velocity are negligible close to the bubble departure (see Eq. (11)).

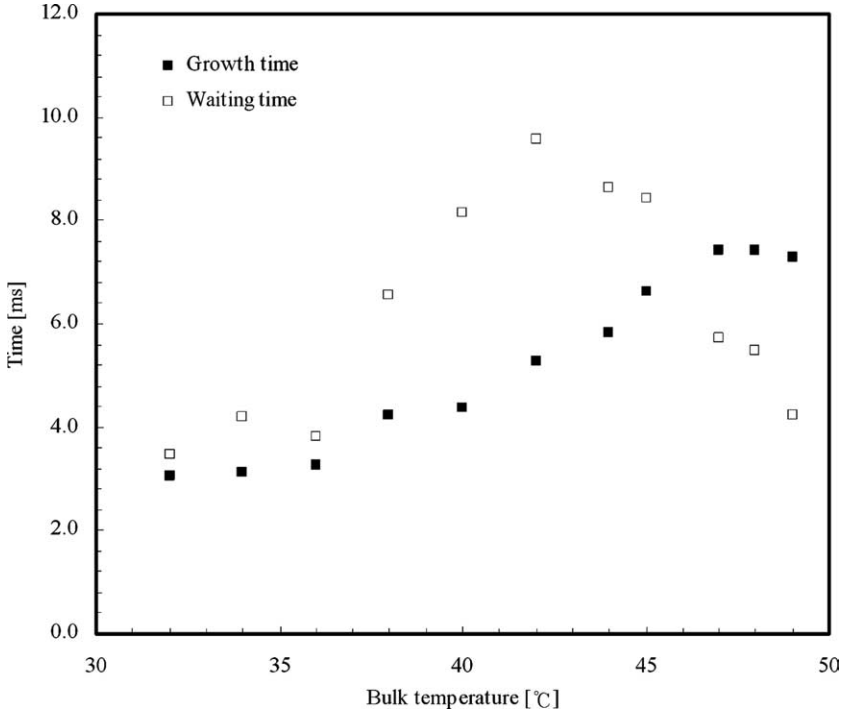

Fig. 9. Waiting and growth times for different pool temperatures.

Therefore

$$\Delta P = \frac{2\sigma}{R_d} \tag{14}$$

Then, the characteristic scales from Eq. (9) can be rewritten as

$$R_c = \frac{\sqrt{27}}{2} Ja\, \alpha \sqrt{\frac{\rho_l R_d}{\sigma}}, \quad t_c = \frac{9}{4} Ja\, \alpha \frac{\rho_l R_d}{\sigma} \tag{15}$$

The characteristic scale of the heat flow rate was obtained from Eq. (5)

$$\dot{q}_c = 4\pi \rho_v h_{fg} R_c^2 \frac{R_c}{t_c} \tag{16}$$

3.4. Bubble growth and heat flow rate behavior

Since the wall temperature was fixed, the Jakob numbers based on the wall and saturation temperatures for all pool temperatures were fixed at 32.4. The characteristic radius and time scales also remained constant for different pool temperatures. These were estimated using Eqs. (13) and (15) for the initial and thermal growth regions, respectively. For saturated condition of a pool temperature of 47 °C, the initial region corresponded to the 1 ms from inception based on the definition proposed by Kim et al. (2004a,b). Fig. 10(a) and (b) showed the dimensionless bubble radius characteristics as functions of the dimensionless time calculated using the estimated characteristic scales using Eqs. (15) and (13), respectively.

The bubble growth rate remained similar for the initial growth region, regardless of the pool temperature. The dimensionless bubble radius (R^+) was proportional to the dimensionless time $t^{+2/3}$, except for pool temperatures less than 40 °C, for which the growth rate decreased from $t^{+2/3}$ to $t^{+1/2}$, as shown in Fig. 10(a). This

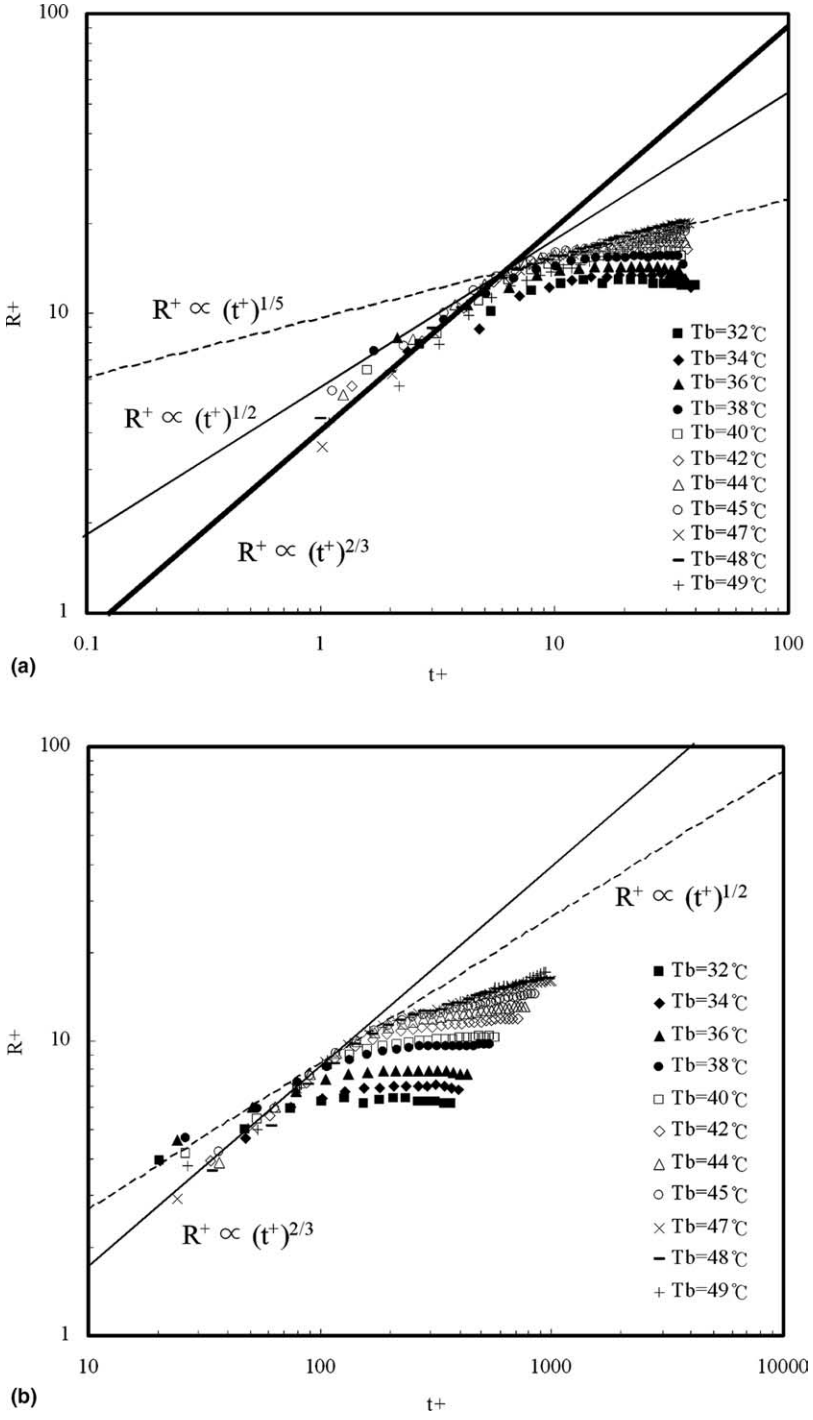

Fig. 10. Bubble growth behavior based on dimensionless scales.

indicates that a characteristic temperature scale that considers the wall and saturation temperatures can describe the initial growth behavior well. For the thermal growth region at a pool temperature of 47 °C, the dimensionless radius R^+ was proportional to dimensionless time $t^{+0.216}$, as expected. The bubble growth rates at pool temperatures of 48 and 49 °C were proportional to $t^{+0.224}$ and $t^{+0.263}$, respectively, as shown in

Fig. 10(b). Nevertheless, these growth rates were still less than $t^{+1/3}$, so the heat flow rate behavior will decrease with growth time, as shown in Fig. 3.

We compared the bubble growth with previous saturated pool boiling experimental results during the initial growth region like Fig. 11(a) because of the growth behavior different with the previous results. In the previous

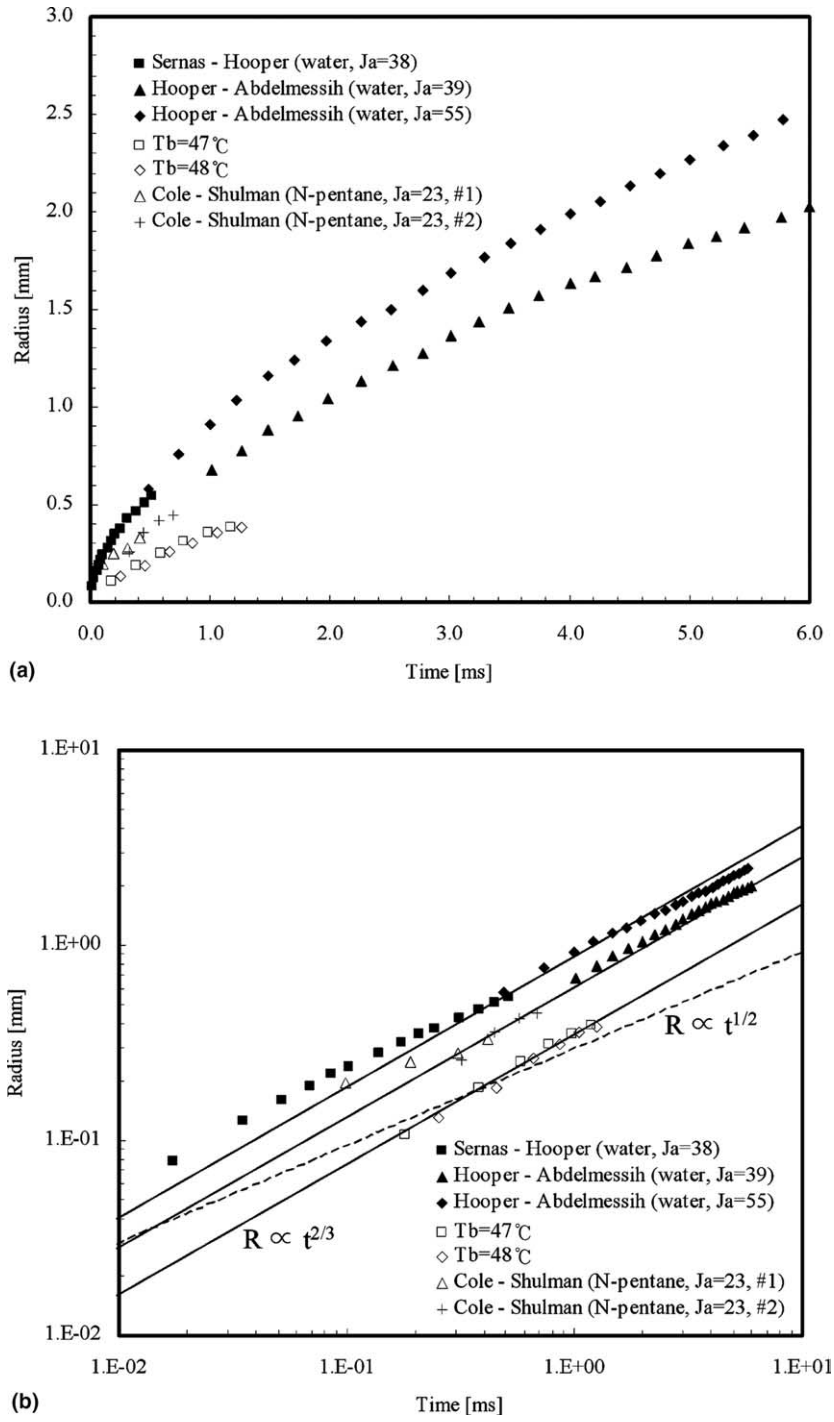

Fig. 11. Comparison of initial bubble growth with previous saturated experimental results.

experiments, water (Sernas and Hooper, 1969; Hooper and Abdelmessih, 1966) and *n*-pentane (Cole and Shulman, 1966) were used as the working fluids. A constant heat flux was applied at the heating surface. Both the present and previous experiments were performed in a pool at saturation temperature under atmospheric pressure. There appears to be a discernable difference between the working fluids. It is not clear how much the wall conditions affect the initial growth rate, but there appears to be no discernable difference between the two different wall conditions. As shown in Fig. 11(b), for saturated nucleate pool boiling, the initial growth rate was proportional to $t^{2/3}$. The heat flow rate increased at first, and then decreased after about 1 ms (see Fig. 7(b)) for our constant wall temperature condition.

Fig. 12 compares our results with previous data scaled using the dimensionless parameters of Eq. (13). The two growth rates described previously are distinguishable in the figure. There was good agreement between the bubble growth in the initial growth region, which was proportional to $t^{+2/3}$, regardless of the working fluids, heating surface conditions, or Jakob number under saturated and ambient pressure conditions. All the results shown in the figure, except those from this study, were performed using a constant heat flux condition. The small amount of initial data scatter might mainly due to the different heating surface conditions or experimental uncertainties near the inception time. The measured heat flow rate close to departure, which was similar to the constant heat flux condition, did not vary significantly, while there were large variations during the initial growth phase. In addition, there were many uncertainties near bubble inception, such as cavity size, inception time, and heater control. The growth rate transition from the initial to thermal growth regions occurred at a dimensionless time of 140.

The results showed that the bubble growth rate was proportional to $t^{+2/3}$ in the initial growth region. This is less than the analytical result of Rayleigh (1917). Rayleigh analyzed the bubble growth rate based on a constant pressure difference between the liquid and vapor bubble. However, the vapor pressure of the bubble decreased as the bubble radius increased with time, as shown in Fig. 13. Therefore, it is possible that the growth rate is less than Rayleigh's result for the initial region. In addition, Mikic et al. (1970) proposed that the bubble radius increased linearly with time for dimensionless time scales much less than 1 ($t^+ \ll 1$). If the same dimensional analyses were applied to the numerical results of Robinson and Judd (2001), the region of t^+ from inception to 0.014 would correspond to the surface tension controlled region, and the region from $0.014 < t^+ < 140$ would correspond to the inertia controlled region, as shown in Fig. 12. Mikic's range for

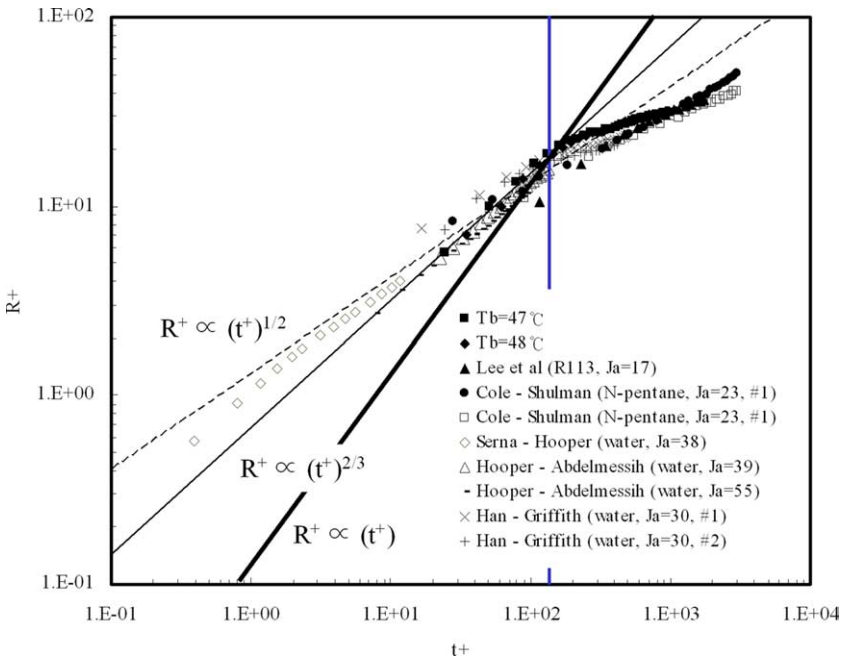

Fig. 12. Initial bubble growth behavior based on dimensionless scales at saturated.

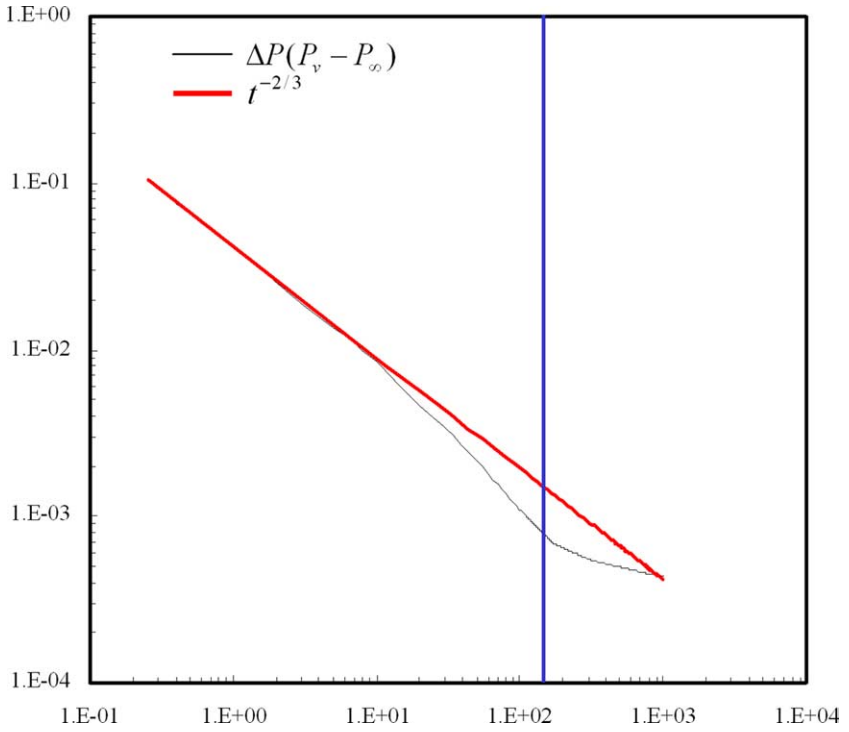

Fig. 13. Variations in the pressure difference to the growth time at saturated.

$t^+ \ll 1$ is also an estimate of the surface tension controlled region. Based on the dimensionless time scale of our results, however, our camera frame rate would have to be increased by 1000 times in order to measure the bubble geometry for R113 in the surface tension controlled region.

We calculated values for each term of the extended Rayleigh equation given in Eq. (11) using the equivalent bubble radius obtained from the captured bubble images. If the growth rate is proportional to $t^{+2/3}$ in the initial growth region, as shown in Fig. 12, the pressure difference will also be proportional to $t^{+2/3}(\Delta P \propto t^{-2/3})$. Fig. 13 shows the characteristics of the total pressure difference between the vapor and the system during the bubble growth as dimensionless scales. The growth rate estimated in the initial region described the growth behavior well. From the results of Fig. 13, we defined the initial growth region as the period of time from inception until the vapor pressure was almost same as the system pressure, following the proposal by Robinson and Judd (2001). Therefore, the length of time required for the initial bubble growth region from inception was approximately 140 dimensionless time units, or about 1.0 ms as dimensional time for R113.

We calculated the required heat flow rate for bubble growth using Eq. (5), and fitted the growth equations for each pool conditions. Then, we integrated the required and measured heat flow rates from inception to departure. The difference between the required and measured heat is shown in Fig. 14. The measured heat was defined as that which was measured using the microscale heater array to maintain the heating surface temperature at a fixed value. When the required heat was less than the measured heat, heat transfer (condensation) loss to the surrounding liquid through the bubble interface occurred at the bubble interface. This decreased bubble size and the required heat flow rate could be much less than the measured heat flow rate for low pool temperatures. When the required heat was greater than the measured heat, heat transfer from the surrounding liquid to the bubble occurred at the bubble interface, providing an interface cooling effect, as proposed by Robinson and Judd (2001). In our experiments, the required and measured heat was balanced when the pool temperature was 40 °C.

We normalized the heat supplied from the heating wall using the total required heat flow rate. As shown in Fig. 15, the heat supplied from the heating wall was roughly 100, 50, and 44% of the required heat for bubble growth for pool temperatures of 40, 47, and 49 °C, respectively. Therefore, when the pool temperature was

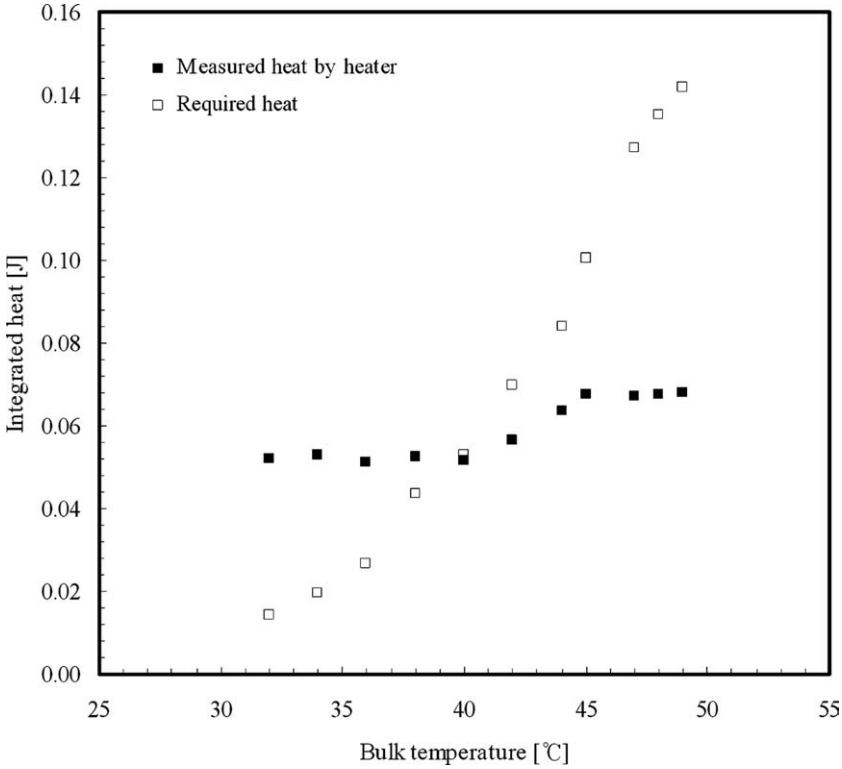

Fig. 14. Heat comparison between measured at wall and required.

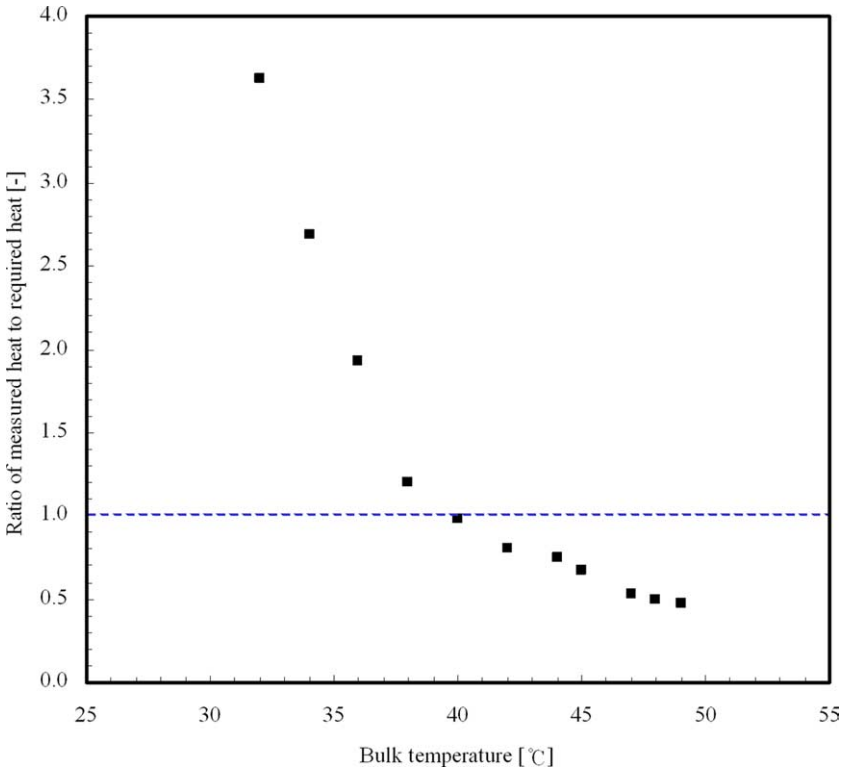

Fig. 15. Comparison of normalized heat between the measured at wall and the required.

increased, the contribution of the instantaneous heat supply from the wall decreased due to more heat supply (or less heat loss) from the surrounding liquid to the bubble. For the saturation temperature, the result was similar with that of Lee et al. (2003a,b).

Koffman and Plesset (1983) reported that a maximum of 50% of the heat flow during bubble growth was transferred due to microlayer evaporation at saturated pool condition. From the bottom view image and heat

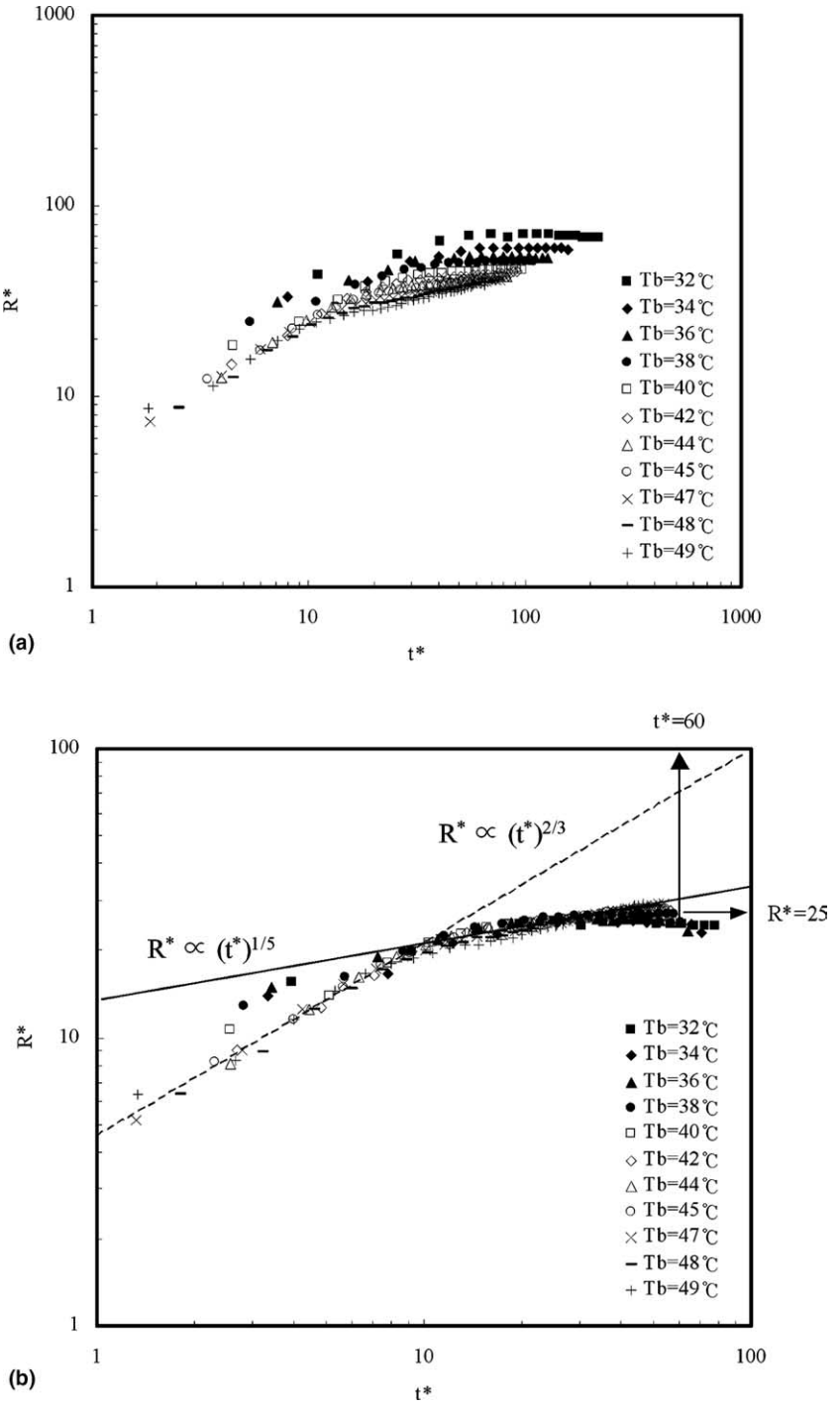

Fig. 16. Dimensionless bubble radius for different pool temperatures using the modified Jakob number.

flow rate data, we observed that the instantaneous heat was transferred through a narrow region near the contact line. Therefore, if a microlayer exists underneath the bubble, most of the measured heat flow rate supplied from the wall will be transferred by microlayer evaporation and Lee et al. (2003a,b) also presented similar results. Additional information about the heat transfer characteristics during single bubble growth presented here can be found in Lee et al. (2003a,b).

The Jakob number remained at 32.4 for all pool temperatures. In order to well consider the effects of the subcooled and superheated pool temperatures in the thermal growth region, we performed a dimensional analysis using a modified Jakob number, $Ja^* = (\rho_l C_{P_l} \Delta T^*)/(\rho_v h_{fg})$, based on a new characteristic temperature rather than, $T_c = \Delta T = T_{wall} - T_{sat}$

$$T_c^* = f(T_{wall}, T_b, T_{sat}) = \beta(T_{wall} - T_{sat}) + (1-\beta)(T_b - T_{sat}) \tag{17}$$

where β is the constant. If $\beta = 1$, the characteristic temperature is the same as the original characteristic temperature, and if $\beta = 0$, the characteristic temperature is the temperature difference between the pool and saturation temperatures. Therefore, the characteristic length and time scales (R^* and t^*) were estimated using Eq. (15) and Ja^*.

We performed a dimensional analysis using modified Jakob numbers ranging from 16.5 ($T_b = 32$ °C) to 23.2 ($T_b = 49$ °C) for various β ranging from 0 to 1. The bubble growth behavior obtained for $\beta = 0.7$ is shown in Fig. 16(b). All thermal growth behaviors were well matched for $\beta = 0.7$ for all pool temperatures. The growth rate in the initial growth region was proportional to $t^{*2/3}$, except when below $Ja^* < 20$ ($T_b < 40$ °C) and the growth rate in the thermal growth region was proportional to $t^{*1/5}$ for all pool temperatures. These results suggest that the wall temperature effect contributed 70% to bubble growth and the pool temperature effect contributed 30%. Additionally, the bubble growth behavior obtained for $\beta = 0.5$ is shown in Fig. 16(a). All thermal growth behaviors were not well matched for $\beta = 0.5$ for all pool temperatures.

Previously, Van Stralen (1966) has extended bubble growth theory to a bubble growing on a heated wall with an exponential radial temperature profile in the liquid. He also assumed that a part of the bubble interface was in the superheated thermal boundary layer as shown in Fig. 17, which he calls the relaxation microlayer. The ratio of the height of the superheated thermal boundary layer thickness (H_T) to the height of the bubble (H^*) is the new parameter (b). Then he performed an experiment with water at atmospheric pressure and calculated the parameter (b) from the bubble growth data. Finally, he showed that the values of b were about 0.7 for water almost same with the result of this study.

Lee et al. (2003a,b) showed that the dimensionless departure radius (R_d^+) was approximately 25, and the dimensionless departure time (t_d^+) was approximately 60, regardless of the boundary conditions or working fluids used for saturated nucleate pool boiling experiments. The results illustrated in Fig. 16(b) show the same characteristics. Using modified values of the dimensionless departure radius and time (R_d^*, t_d^*), the following predictions are obtained:

$$\begin{aligned} R_d^* &= \frac{R_d}{\frac{\sqrt{27}}{2} Ja^* \alpha \sqrt{\frac{\rho_l R_d}{\sigma}}} = 25, \\ t_d^* &= \frac{R_d}{\frac{9}{4} Ja^* \alpha \frac{\rho_l R_d}{\sigma}} = 60, \end{aligned} \tag{18}$$

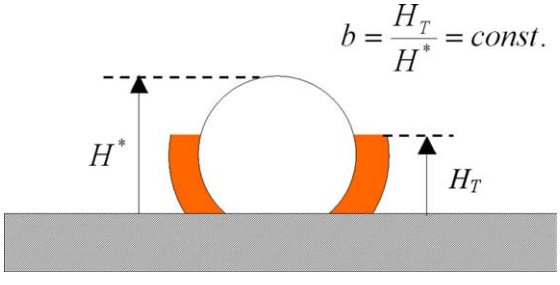

Fig. 17. Relaxation microlayer of Van Stralen (1966).

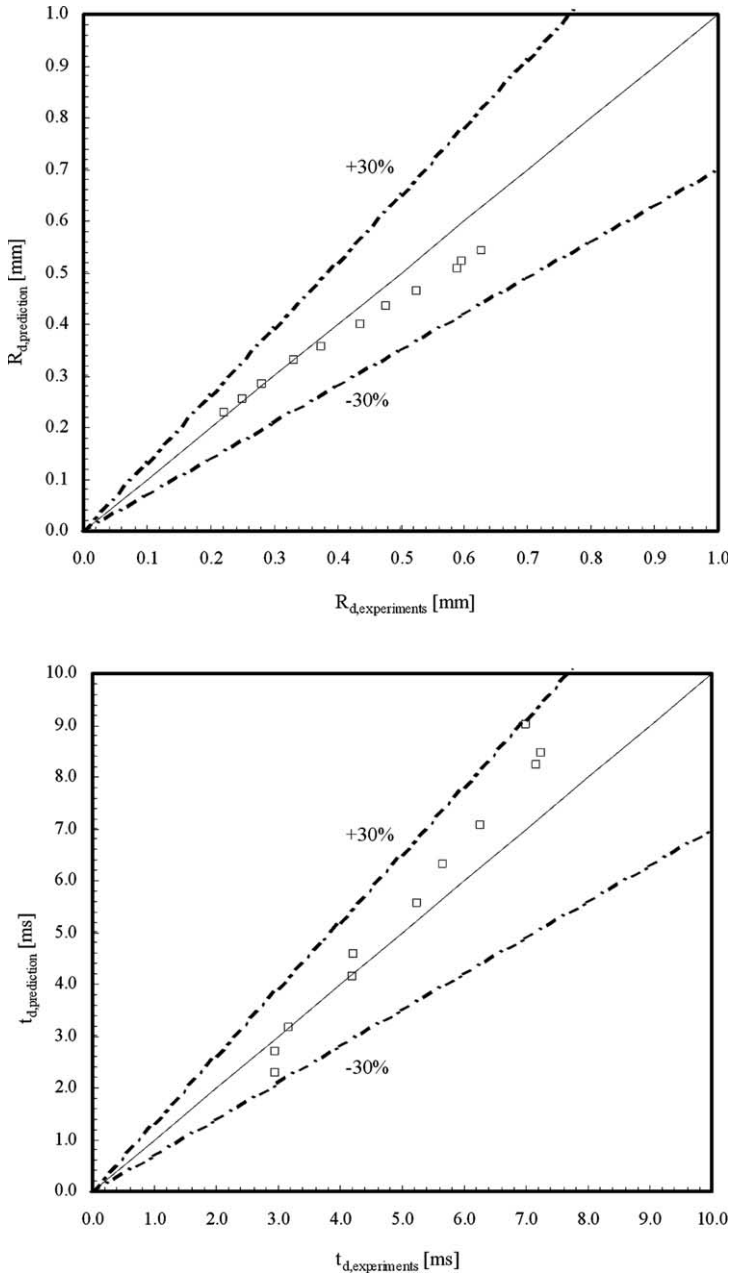

Fig. 18. Comparison of the predicted and experimental departure radius and time.

$$R_d = \left[\frac{25}{2}\sqrt{27}Ja^*\alpha\sqrt{\frac{\rho_l}{\sigma}}\right]^2,$$
$$t_d = 135Ja^*\alpha\frac{\rho_l R_d}{\sigma}. \tag{19}$$

Fig. 18 compares the predicted departure radius and time with the experimental results. The departure radius and time were predicted with less than a 30% error.

4. Conclusions

A quantitative analysis of single bubble growth during subcooled, saturated, and superheated nucleate pool boiling was performed with a constant wall temperature. The wall temperature was controlled precisely using a microscale heater array, and the local heat flow rate was measured at a high temporal resolution. Time-triggered high-speed CCD images were captured at a sampling rate of 5000 Hz to analyze bubble motion.

The captured images showed a spheroidal bubble during growth. The equivalent radius of a sphere with the same volume produced a small error for the shape assumption. Using our measured results, we quantified showed the bubble growth rate and geometry using bubble images for subcooled, saturated, and superheated pool conditions with fixed wall temperature. We also showed the required and measured heat flow rate characteristics for all pool temperature conditions.

The bubble growth behavior during subcooled, saturated, and superheated pool boiling was analyzed using a modified Jakob number that we defined. The dimensionless parameters of time and bubble radius characterized the bubble growth behavior well using a modified Jakob number with $\beta = 0.7$. In the initial growth region, the growth rate was proportional to $(t^*)^{2/3}$ for all pool temperatures except when $Ja^* < 20$ ($T_b < 40$ °C). In the thermal growth region, the growth rate was proportional to $(t^*)^{1/5}$ for all pool temperatures.

Acknowledgements

This work was supported by the Ministry of Science and Technology of Korea through the National Research Laboratory program. The authors thank Prof. Jungho Kim and Dr. Sung Won Bae for providing the basic design of the microscale heater array, including its controller, and the Samsung Advanced Institute of Technology for fabricating the microscale heater array.

References

Bae, S.W., Kim, J., Kim, M.H., 1999. Improved technique to measure time- and space- resolved heat transfer under single bubbles during saturated pool boiling of FC-72. Exp. Heat Transfer 12, 265–279.

Cole, R., Shulman, H.L., 1966. Bubble growth rates at high Jakob numbers. Int. J. Heat Mass Transfer 9, 1377–1390.

Coleman, W.H., Steele, W.G., 1989. Experimentation and Uncertainty Analysis for Engineers. John-Wiley & Sons.

Demiray, F., Kim, J., 2003. Heat transfer from a single nucleation site during pool boiling of FC-72. Int. Conf. Boiling Heat Transfer.

Dergarabedian, P., 1960. Observations on bubble growths in various superheated liquids. J. Fluid Mech. 9, 39–48.

Forster, H.K., Zuber, N., 1954. Growth of a vapor bubble in a superheated liquid. J. Appl. Phys. 25, 474–478.

Han, C.H., Griffith, P., 1965. The mechanism of heat transfer in nucleate pool boiling—part I bubble initiation, growth and departure. Int. J. Heat Mass Transfer 8, 887–904.

Hooper, F.C., Abdelmessih, A.H., 1966. In: 3rd Intl. Heat Tr. Conf. Chicago: This is cited in the paper titled A theoretical study on bubble growth in constant and time-dependent pressure fields by Theofanous, T., Biasi, L., Isbin, H.S., Fauske, H., (1969). Chem. Eng. Sci. vol. 24, pp. 885–897.

Kim, J., Benton, J.F., Wisniewski, D., 2002. Pool boiling heat transfer on small heaters: effect of gravity and subcooling. Int. J. Heat Mass Transfer 45, 3919–3932.

Kim, J., Lee, H.C., Oh, B.D., Kim, M.H., 2004a. Effects of bubble shape assumption on single bubble growth behavior in nucleate pool boiling. J. Flow Visualization Image Process. 11, 73–87.

Kim, J., Lee, H.C., Oh, B.D., Kim, M.H., 2004b. Study on the Initial Growth of Single Bubble at Saturated Nucleate Boiling. ICMF 2004 in Yokohama.

Koffman, L.D., Plesset, M.S., 1983. Experimental observation of the microlayer in vapor bubble growth on a heated solid. J. Heat Transfer 105, 625–632.

Lee, H.C., Oh, B.D., Bae, S.W., Kim, M.H., 2003a. Single bubble growth in saturated pool boiling on a constant wall temperature surface. Int. J. Multiphase Flow 29, 1857–1874.

Lee, H.C., Oh, B.D., Bae, S.W., Kim, M.H., Lee, J.Y., Song, I.S., 2003b. Partial nucleate boiling on the microscale heater maintaining constant wall temperature. J. Nucl. Sci. Technol. 40, 768–774.

Lee, H.C., Kim, J., Oh, B.D., Kim, M.H., 2004. Single bubble growth in saturated pool boiling of binary mixtues. Int. J. Multiphase Flow 30, 697–710.

Lien, Y., 1969. Bubble Growth Rates at Reduced Pressure, ScdR. Thesis, Mechanical Engineering Department, MIT.

Mikic, B.B., Rohsenow, W.M., 1969. Bubble growth rates in non-uniform temperature field. Progr. Heat Mass Transfer II, 283–293.

Mikic, B.B., Rohsenow, W.M., Griffith, P., 1970. On bubble growth rates. Int. J. Heat Mass Transfer 13, 657–666.

Plesset, M.S., Zwick, S.A., 1954. The growth of vapor bubbles in superheated liquids. J. Appl. Phys. 25, 493–500.

Rayleigh, J.W.S., 1917. On the pressure developed in a liquid during the collapse of a spherical cavity. Philos Mag 34, 94–98, This is cited in the book titled Boiling Phenomena by S. Van Stralen, 1979, McGraw-Hill.

Robinson, A.J., Judd, R.L., 2001. Bubble growth in a uniform and spatially distributed temperature field. Int. J. Heat Mass Transfer 44, 2699–2710.

Rule, T.D., Kim, J., 1999. Heat transfer behavior on small horizontal heaters during pool boiling. J. Heat Transfer 121, 386–393.

Rule, T.D., Kim, J., Kalkur, T.S., 1998. Design, construction and qualification of a microscale heater array for use in boiling heat transfer. NASA/CR-1998-207407.

Saddy, M., Jameson, G.J., 1971. Prediction of departure diameter and bubble frequency in nucleate boiling in uniformly superheated liquids. Int. J. Heat Mass Transfer 14, 1771–1783.

Sernas, V., Hooper, F.C., 1969. The initial vapor bubble growth on a heated wall during nucleate boiling. Int. J. Heat Mass Transfer 12, 1627–1639.

Van Stralen, S.J.D., 1966. The mechanism of nucleate boiling in pure liquids and in binary mixtures—part I. Int. J. Heat Mass Transfer 9, 995–1020.

Van Stranlen, S.J.D., Sohal, M.S., Cole, R., Sluyter, W.M., 1975. Bubble growth rates in pure and binary systems: combined effect of relaxation and evaporation microlayers. Int. J. Heat Mass Transfer 18, 453–467.

Zuber, N., 1961. The dynamics of vapor bubbles in nonuniform temperature fields. Int. J. Heat Mass Transfer 2, 83–98.